AERODYNAMICS OF A ROLLING AIRFRAME MISSILE*

L. E. Tisserand
The Johns Hopkins University/Applied Physics Laboratory
Laurel, Maryland

14 May 81

ABSTRACT

For guidance-related reasons, there is considerable interest in rolling missiles having single-plane steering capability. To aid the aerodynamic design of these airframes, a unique investigation into the aerodynamics of a rolling, steering missile has been carried out. It represents the first known attempt to measure in a wind tunnel the aerodynamic forces and moments that act on a spinning body-canard-tail configuration that exercises canard steering in phase with body roll position.

Measurements were made with the model spinning at steady-state roll rates ranging from 15 to 40 Hz over an angle-of-attack range up to about 16°.

This short, exploratory investigation has demonstrated that a better understanding and a more complete definition of the aerodynamics of rolling, steering vehicles can be developed by way of simulative wind-tunnel testing.

INTRODUCTION

In mid-December 1978, wind tunnel tests were conducted using the newly fabricated model of a Rolling Airframe Missile. The Applied Physics Laboratory planned[1] and conducted the testing for the Navy under APL subcontract with the Vought Corporation, High Speed Wind Tunnel. General Dynamics, Pomona Division, designed and fabricated the test item.[2,3,4]

The purpose of this wind-tunnel investigation was to gain a better understanding of the configuration's aerodynamic characteristics, under proper simulative conditions, that would lead to the development of better predictive capabilities. Prior to this effort, aerodynamic characteristics used in designing and evaluating rolling, steering missiles have been derived from wind tunnel data collected on nonspinning models and from the cumulative experiences gained from analyses of flight test data. Those aerodynamic descriptions of rolling airframes emphasize their longitudinal stability and control characteristics but ignore the likelihood of induced side forces and yawing moments.

*The work reported in this paper was supported by NAVSEA, PMS-404-50, under Contract N00017-72-C-4401, Task A3B0

This exploratory test was limited purposely to 35-hours of test time. It represents Phase One of a two-phase wind-tunnel investigation into the aerodynamics of the rolling, steering airframe. The objectives of this short test were to check out the test item, test procedures and data acquisition, and to probe the aerodynamics of the configuration under dynamic-flight conditions at a representative transonic and supersonic speed. It was proposed that, after an evaluation of all aspects of this test, a second tunnel entry would be made to fully document the aerodynamics of the configuration throughout its performance envelope, and to conduct configurational breakdown investigations appropriate to the identification and sizing of relevant aerodynamic causes and effects.

This first phase of the proposed test program was a success. The test data have been evaluated and the results documented.[6]

SYMBOLS AND NOMENCLATURE

The aerodynamic forces and moments presented herein are referred to an axes system of rectangular coordinates (x,y,z) that pitches with the missile but does not roll with the missile, and does not roll to the angular orientation for the occurrence of peak-steering deflection. The flight-path velocity vector is denoted by V with projections u, v, w on the x,y,z-axis respectively ($v \equiv 0$ for the axes system selected herein). The positive sense of the velocity components, force and moment coefficients, and steering-control deflection are shown on the next page. Definitions of symbols are:

$C_A, C_Y, C_N,$ C_ℓ, C_m, C_n	orthogonal set of aerodynamic force and moment coefficients: $C_A = -F_x/qS$, $C_Y = F_y/qS$, $C_N = -F_z/qS$, $C_\ell = M_x/qSd$ $C_m = M_y/qSd$, $C_n = M_z/qSd$
d	reference length, body diameter (inches)
F_x, F_y, F_z M_x, M_y, M_z	projections of the total aerodynamic force (lbs) and total aerodynamic moment (in-lbs) onto the non-rolling x, y, z-axis respectively
i	steering deflection amplitude, $i > 0$ increases α and $i < 0$ decreases α [an observer riding in the non-rolling axes system will see the instantaneous steering deflection vary as $i \lvert \cos \phi \rvert$; an observer riding in the rolling body-fixed axes system will see the instantaneous steering deflection vary as $i \cos \phi$]

M — Mach number

MRC — moment reference center located seven model diameters downstream of body nose tip

q — dynamic pressure (psf)

S — reference area, body cross-sectional area, $\pi d^2/4$ (sq. ft)

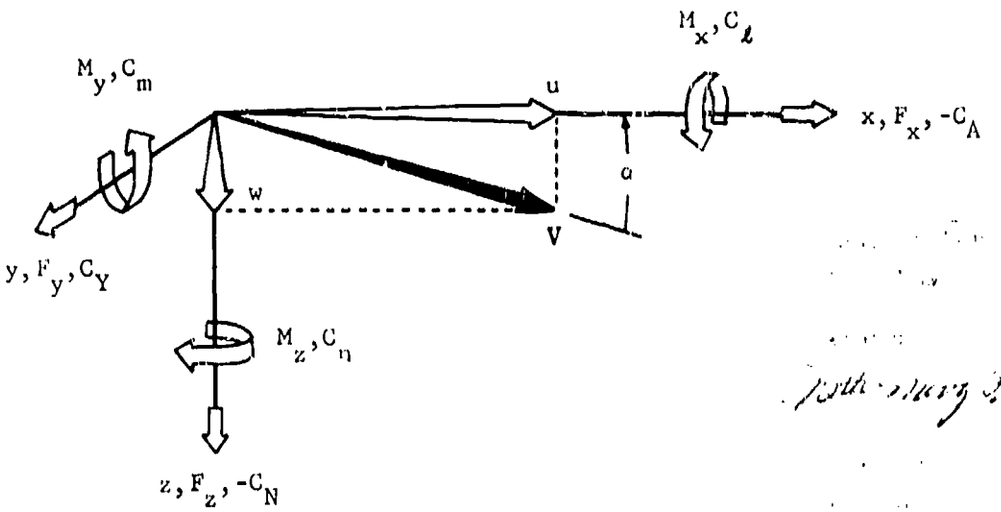

XCP — longitudinal center of pressure (used to indicate the resultant center-of-pressure location for the normal force coefficient where body station is given in model diameters measured downstream from nose tip)

α — total angle of attack (deg) measured between the total velocity vector (V) and the centerline of the missile (x-axis): $\alpha = \arctan(w/u)$

ϕ — when $\dot{\phi} = 0$, ϕ is the aerodynamic roll angle (deg) measured from the angle-of-attack plane (defined by the total velocity vector and the centerline of the missile) to the centerline of the reference leeward canard; when $\dot{\phi} \neq 0$, ϕ is the steering-control direction defined as the angle (deg) measured from the angle-of-attack plane to the roll attitude for the occurrence of peak-steering deflection.

$\dot{\phi}$ — roll rate (Hz); $\dot{\phi} > 0$ is clockwise spin looking upstream

$\dot{\phi}d/2V$	spin parameter (radians)
δ	differential deflection angles (deg) set on lifting panels
cw, ccw	clockwise, counterclockwise
ζ	nonzero value of C_Y at $\alpha = 0°$
ξ	nonzero value of C_n at $\alpha = 0°$
∂	partial differentiation as in $\partial C_Y/\partial\alpha$

TEST ITEM

The configuration tested is shown in Figure 1. The model is 42.408 inches long and its outer diameter is 1.925 inches. The nose section consists of a hemispheric nose stepped into a conical-transition section leading to the cylindrical body. Two hemispherically-tipped antennas are mounted on the transition section in line with the two fixed, rectangular-planform canards that are canted differentially ($\delta = -0.75°$) for the intended purpose of supplementing aerodynamic rolling moment. The two steering canards have a delta planform with 45° leading-edge sweep. Provisions exist for testing steering-deflection amplitudes of 0°, ±5°, ±10°, ±15° or ±20°. Four like tail panels are mounted on a cylindrical sleeve which is slip-fitted over, and fastened to, the cylindrical afterbody. The cruciform tail arrangement is interdigitated at 45° relative to the canard panels. Asymmetric wedging of the tail leading edges yields a camber effect, and small flap-type tabs at the trailing edges are deflected differentially ($\delta = -7.5°$) to produce aerodynamic roll-driving moment. The base is flared.

A special sting support was designed and fabricated to be compatible with the model's large length-to-diameter ratio. Packaged inside the model are: (a) a five-component strain guage balance to measure the orthogonal aerodynamic forces (less drag) and moments that act on the model, (b) a DC motor to provide roll torque supplemental to aerodynamic roll-driving moment, and (c) an interchangeable steering cam to produce mechanically sinusoidal deflection of the steering canards in phase with body roll position. The sting support, balance, motor casing, and cam are locked together as one unit that does not spin; the model is slip-fitted over, and fastened to, a spin-bearing case that is free to rotate. The roll rate of the model can be controlled remotely by regulating the power supply to the torque motor.

Pretests showed the model's mass asymmetry in roll is quite small, and the effects of motor-generated heat and magnetic fields on the performance of the balance are negligible. Resonant frequencies of the cantilevered model-balance-sting assembly are 12, 22 and 24 Hz.

TEST CONDITIONS

A dynamic variable to be duplicated in tunnel testing is the missile's spin parameter, $\dot{\phi}d/2V$, rather than the missile's roll rate, $\dot{\phi}$. Hence, to simulate properly the flight conditions associated with missile roll rates of 8 to 15 Hz, it is necessary for the 0.385-scale model to experience steady state roll rates of 15 to 30 Hz. Resonant frequencies within the simulative range of model roll rates would have been a serious problem had it not been for the ability to control the roll rate of the model remotely. Figure 2 shows, for Mach 1.2 and 2.5, the model roll rates tested and the equivalent missile roll rates (evaluated at sea level) determined from the equivalence of the spin parameter.

Measurements were taken under conditions of pitch and pause at the nominal angles of attack of -2°, 0°, 2°, 4°, 6°, . . ., 16°. The effects of data sampling rate, roll rate, Reynolds number, Mach number, and steering control (directed "in" and "out" of the angle-of-attack plane) on the configuration's rigid-body aerodynamics were examined.

RESULTS

A pretest calibration of the balance provided a measure of the basic, static accuracy of the instrument. The root-mean-square variations in the balance-measured forces and moments are shown in subsequent plots of coefficient data. Evaluation of all test results has shown the repeatability of balance measurements is excellent and the measurements satisfy principles of symmetry when required. These important data properties are used as justification to define some coefficient behavior to finer precision than the advertised accuracy of the balance.

Some pertinent results follow. Additional information and detail are given in the final report.[b]

EFFECTS OF ROLL RATE AND DATA SAMPLING RATE

Tests were made holding the model roll rate constant at -17, -30 or -40 Hz. At each pause, 48 data points were recorded at the rate of 240 data points per second. This yielded about 16 data points per one revolution of the model when $\dot{\phi}$ = -17 Hz, 8 data points per revolution when $\dot{\phi}$ = -30 Hz, and 6 data points per revolution when $\dot{\phi}$ = -40 Hz. In the data reduction program, these 48 lines of coefficients were divided into four equal groups, and for each group, a mean value and standard deviation were computed for each coefficient. Hence, in the figures, four mean values could appear at each condition of pause; less than four plotted points indicates no significant difference in some of the coefficient's computed mean values.

Figures 3, 4 and 5 show, for Mach 2.51, the effect of roll rate on the aerodynamic forces and moments that act on the configuration. It is evident that normal force and pitching moment coefficients are not sensitive to the roll rates tested. The data allow smooth fairings without anomalies.

The induced side force and yawing moment coefficients, Figure 5, show a dependence on roll rate and angle of attack. Although these forces and moments induced out of the plane of maneuver are small compared to the normal force and its associated pitching moment, their appearance was not unexpected.[1] If these fairings of induced coefficients are shifted to a common origin, it is possible to combine the slopes for low angles of attack into second-order expressions of the form,

$$\frac{\partial^2 C_Y}{\partial \alpha \, \partial P} \quad \text{and} \quad \frac{\partial^2 C_n}{\partial \alpha \, \partial P} \quad \text{for } 0° \leq \alpha < 4°, \text{ where } P = \frac{\dot{\phi} d}{2V} ,$$

which are used commonly to describe the behavior of Magnus effects on bodies of revolution. It is not proposed that Magnus forces acting on the model's body are the only contributors to the configuration's induced side force and yawing moment characteristics.[6]

Tests were made to determine the effect of data sampling rate on aerodynamic output. Holding $\dot{\phi}$ = - 30 Hz, measurements were taken over the angle of attack range -2° to 16° using data sampling rates of 80, 240 and 320 data points per second respectively. Comparison of results obtained indicates no measurable effect of data sampling rate on the recorded aerodynamic forces or moments. One test run was made with the balance rolled to a different orientation relative to the angle-of-attack plane, and it is significant that the balance output (when resolved to the axes system adopted herein) duplicate the results for $\dot{\phi}$ = -30 Hz presented in Figures 3, 4, and 5.

EFFECTS OF STEERING CONTROL DIRECTED IN THE ANGLE OF ATTACK PLANE

The results presented in this section are for conditions where peak-steering deflection occurs as the steering canards become normal to the angle-of-attack plane, i.e., ϕ = 0°.

Longitudinal Stability and Control Characteristics and Induced Side Force and Yawing Moment Coefficients

Figures 6 and 7 show, for Mach 2.51, the effect of steering-deflection amplitude on the contributers to longitudinal stability and control. The variations of normal force and pitching moment coefficients with angle of attack and steering control show remarkably smooth and consistent behavior. Figure 8 shows the behavior of the induced side force and yawing moment characteristics. The fairings for zero incidence are the same as shown earlier and their nonzero intercepts with the ordinate are designated, for purposes of discussion, as Zeta (ζ_1) and Xi (ξ_1). At zero angle of attack, principles of symmetry require that the incremental force and incremental moment resulting from plus and minus steering deflection to be equal and opposite; this condition is satisfied if increments are measured from ζ_1 and ξ_1 respectively.

The test data should also image about zero angle of attack; i.e., C_Y ($\alpha = j$, $i = k$) $\equiv -C_Y$ ($\alpha = -j$, $i = -k$) and C_n ($\alpha = j$, $i = k$) $\equiv -C_n$ ($\alpha = -j$, $i = -k$). These conditions are satisfied (for the range of data taken) when the origins of the plots are shifted (without rotation) to ζ_1 and ξ_1 respectively.

Figures 9, 10 and 11 show, for Mach 1.19, the effects of angle of attack and steering-deflection amplitude on the force and moment coefficients. Measurements taken with a substantial increase in Reynolds number show no observable change in normal force coefficient and a 0.2-diameter upstream shift in longitudinal center of pressure throughout the angle-of-attack range tested. Due to the nature of transonic flowfields, it was expected that measurements taken at Mach 1.19 would indicate some abrupt changes in the components of the aerodynamic force and moment coefficients; however, it can be observed that the normal force and pitching moment fairings are without anomalies.

Tests were conducted with the direction of spin reversed. For the forces and moments induced out of the maneuver plane to be real and aerodynamic in origin, these coefficients must change sign when spin direction is reversed, and must image about the abscissa or a line parallel to the abscissa. In Run No. 45, the model was spun in the clockwise direction looking upstream. The tail-tabs settings were not reversed, nor was the differential cant on the rectangular canards; hence, the test setup for Run No. 45 is similar but not identical to that of No. 44. The torque motor was used to override the aerodynamic roll-driving moment, roll-damping moment and bearing friction, and as a result, the motor could not produce a steady-state roll rate larger than +15 Hz (cw). Nevertheless, comparisons of normal force and pitching moment coefficients (Figures 9 and 10) from Run No. 44 and 45 show good agreement. Figure 11 compares the measured side force and yawing moment coefficients when roll direction is reversed. The results show clearly that both side force and yawing moment reverse sign and exhibit elements of symmetry when viewed about new abscissas drawn through ζ_2 and ξ_2. Since the magnitude of the roll rates differ, mirror images of the coefficient traces would not be expected.

Plans to interchange the model's tail assembly with an extra assembly preset to produce near identical test conditions for clockwise and counterclockwise spin were not carried out due to an unexpected installation problem.

Transonic tests were made holding angle of attack constant (0°, 4° and 8°) while increasing Mach number from 0.6 to 1.10. Roll rate was - 30 Hz. These Mach number sweeps provided some valuable information about the configuration's low-speed aerodynamics and were appropriate to this probing investigation. Measurements taken under conditions of pause yield smooth fairings for the normal and side force coefficients and for the pitching and yawing moment coefficients. It is significant that the side force and yawing moment coefficients obtained at $\alpha = 3°$ with clockwise spin ($\dot{\phi} = +25 \rightarrow +12$ Hz as $M = 0.6 \rightarrow 1.1$) are opposite in sign to those obtained at $\alpha = 8°$ with $\dot{\phi} = -30$ Hz, but their magnitudes differ (note that deflections on roll producing surfaces were not reversed).

Aerodynamic Roll Driving and
Roll Damping Characteristics

It was planned to evaluate the aerodynamic roll-driving characteristics from nonspin test data. Under these conditions, measurements obtained from the balance roll gauge provide the summations of all roll moments resulting from differential deflection on the nonsteering canards (when installed), asymmetric wedging of tail leading edges, tail-tab deflections, and canard-to-tail interferences.

It was planned to evaluate roll-damping characteristics by solving the one-degree-of-freedom equation of motion in roll:

$$I\ddot{\phi} = C_{\ell}\, qSd + C_{\ell_{(\dot{\phi}d/2V)}} \frac{\dot{\phi}d}{2V}\, qSd.$$

The roll-rate feedback loop in the motor controller maintained very accurately a constant roll rate during the data-recording intervals; therefore, steady-state conditions are satisfied. Motor current was recorded, and using a pre-test calibration curve of current versus torque, data reduction provided a printout of motor torque coefficient. There is, of course, friction in the spin-bearing case that acts always to oppose model rotation. The summation of torques that act on the model can be written as:

$$C_{\ell_{aero}} - C_{\ell_{friction}} + C_{\ell_{motor}} + C_{\ell_{(\dot{\phi}d/2V)}} \frac{\dot{\phi}d}{2V} = 0$$

or, with some approximation, as

$$C_{\ell_{aero}} - C_{\ell_{balance}} + C_{\ell_{(\dot{\phi}d/2V)}} \frac{\dot{\phi}d}{2V} = 0$$

where, because of motor losses, $|C_{\ell_{bal}}| \geq |-C_{\ell_{friction}} + C_{\ell_{motor}}|$.

The aerodynamic roll-driving coefficients were determined from angle-of-attack sweeps conducted at selected roll attitudes without spin. For given angles of attack, the rolling moment coefficients obtained at different roll angles with $i = 0°$ were averaged, and these mean values were taken to be representative of the model's aerodynamic roll-driving moment ($C_{\ell_{aero}}$) when spinning.

Aerodynamic roll-damping coefficients calculated from the equation of motion in roll under steady-state conditions are presented in Figure 12 for Mach 2.51. These computed roll-damping derivatives show a decreasing trend for the increasing roll rates tested. Also, these roll-damping derivatives exhibit an apparent dependence on steering-deflection amplitude at low angles of attack.

The orderly dependence of the computed damping coefficients on steering deflection forces reconsideration of the assumption made in these calculations, namely, that the roll-driving coefficients determined from static test data when i = 0°are independent of spin parameter and steering-deflection amplitude. Perhaps roll-driving moment, or r ll-damping moment, or both, depend on spin parameter and steering control.

Aerodynamic roll-driving and roll-damping coefficients deduced from test data collected in the transonic Mach sweeps with i = 0°are well behaved and exhibit expected trends.

CONFIGURATIONAL BREAKDOWN TESTS

Since this was an exploratory investigation, a few tests were made with some model components removed. With the rectangular-planform canards removed, tests with and without spin were carried out at Mach 1.19 and 2.51. A significant result obtained is that the rectangular canards, canted differentially to produce an increase in net roll-driving moment to offset their contribution to total roll-damping moment, induce a nulling increment of roll-reversal moment[7] on the downstream tails. Tests made at Mach 1.19 with both the rectangular canards and tails removed give further insight into the configurational contributors to both pitch and yaw aerodynamics, and offer additional evidence that steering-deflection amplitude affects roll damping.

EFFECT OF STEERING CONTROL DIRECTED OUT OF THE ANGLE OF ATTACK PLANE

The flight vehicle will respond to guidance called-for maneuvers directed in or out of the instantaneous angle-of-attack plane by causing the steering deflection amplitude to occur in or out of the angle-of-attack plane. Tests were made to determine the effect on maneuver force and its associated moment characteristics due to steering-deflection amplitudes of 10° and 20° directed to roll attitudes of 0°, -22.5° and -45°. The brevity of the tunnel test limited this portion of the study to Mach 2.51.

Viewing collectively the results obtained, it is concluded that the effect of directing steering control out of the angle-of-attack plane can be approximated, for the conditions tested, by directing the control-force increments and control-moment increments obtained when $\emptyset$ = 0° to the new steering direction, then resolving these increments back to the nonrolling axes system used herein. The accuracy of this procedure (exact at zero angle of attack) deteriates somewhat as angle of attack increases.

Evaluation of the test data indicates that steering-control direction affects substantially the aerodynamic contributors to roll characteristics. It is deduced that steering control directed out of the angle-of-attack plane induces a net change in roll-driving moment somewhat like the roll moments induced by roll-stabilized missiles with vertical tails deflected to port or starboard. For the rolling airframe, however, the induced roll-moment increments (dependent on steering amplitude and direction) will increase or decrease the airframe's roll-driving moment (ccw) depending on whether nose-up steering control is directed to the starboard side or port side respectively.

CONCLUSIONS

The normal force and pitching moment data provide smooth definitions of the configuration's longitudinal stability and control characteristics. These forces and moments are not sensitive to the values of spin parameters tested.

Small side forces and associated yawing moments, induced out of the plane of maneuver, show dependence on Mach number, angle of attack, steering-control amplitude and direction, and spin parameter. Before this test, aerodynamic descriptions of rolling, steering airframes omitted aerodynamics induced in the yaw plane because there were no systematic data from experiment on which to base predictions. The importance of these induced side forces and yawing moments to the airframe's flight behavior can be determined from dynamic-flight simulations.

Results show that steering control directed in or out of the angle-of-attack plane affect the aerodynamic contributors to roll characteristics.

REFERENCES

1. L. E. Tisserand, "Test Plan for Wind Tunnel Investigation of the 0.385-Scale ASMD Block I Rolling, Steering Airframe - Phase One (U)," (Unclassified), APL/JHU Internal Memorandum BFD-1-77-032, 30 November 1977.

2. H. Beutel, "ASMD Wind Tunnel Model Design (U)," (Unclassified), General Dynamics Pomona Division, Technical Memorandum 6-420-615, 14 November 1978.

3. F. Shum, "ASMD Wind Tunnel Model Controller (U)," (Unclassified), General Dynamics Pomona Division, Technical Memorandum 6-420-594, September 1978.

4. F. D. Fernandes, "Normal Force and Pitching Moment Coefficients for ASMD Block I with 3-Inch Body Spacer (U)," (Unclassified), General Dynamics, Pomona Division, Technical Design Information 6-332-101.53-59, 19 May 1977.

5. L. E. Tisserand, "Wind Tunnel Investigation by JHU/APL of the 0.385-Scale Block I Rolling Airframe Missile -- Results From Phase One Testing (U)," (Unclassified), APL/JHU Internal Memorandum BFD-1-79-012, 31 July 1979.

6. J. C. Uselton and J. B. Carmon, "A Study of the Magnus Effects on a Sounding Rocket at Supersonic Speeds," Journal of Spacecraft and Rockets, Vol. 8, No. 1, January 1971, pp. 28-34.

7. A. R Eaton, Jr., "Experimental Investigations of Roll-Reversal Effects for Generalized Missile Configurations at Supersonic Velocities," Bumblebee Aerodynamics Symposium, 4-5 November 1948, pp. 237-265.

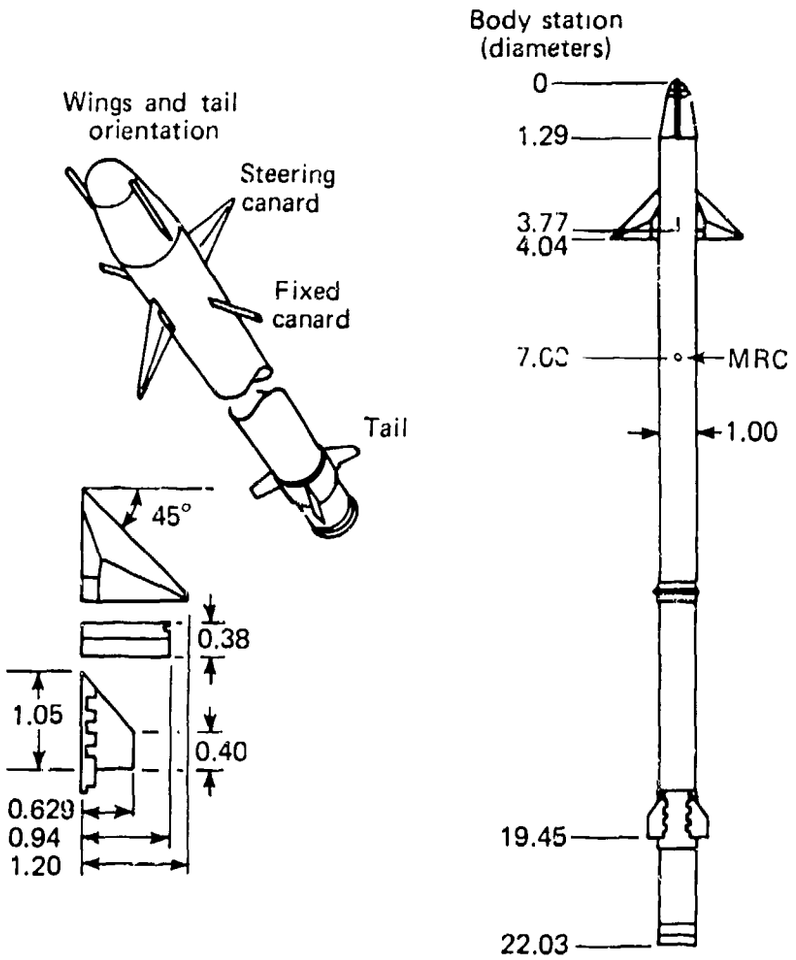

Note: Dimensions normalized with body diameter (1.92 in.)

Fig. 1 Sketch of external configuration.

(a) Mach 2.51

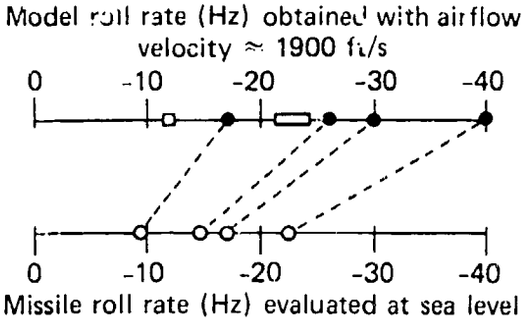

(b) Mach 1.19

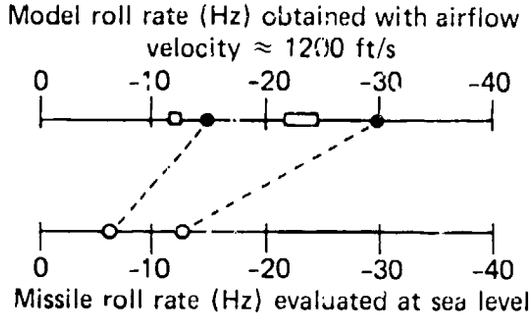

Fig. 2 Model roll rates tested and equivalent missile roll rates.

M = 2.51

Sym	Run No.	$\dot{\phi}$ (Hz)	$\dot{\phi}$d/2V (rad)	Re x 10^{-6} (per ft)	i (deg)	Data sampling (pts/sec)
△	7	-17	-0.0046	8.8	0	240
○	5	-30	-0.0080	8.3	0	240
●	5	-9	-0.0024	8.3	0	240
□	6	-40	-0.0108	8.9	0	240

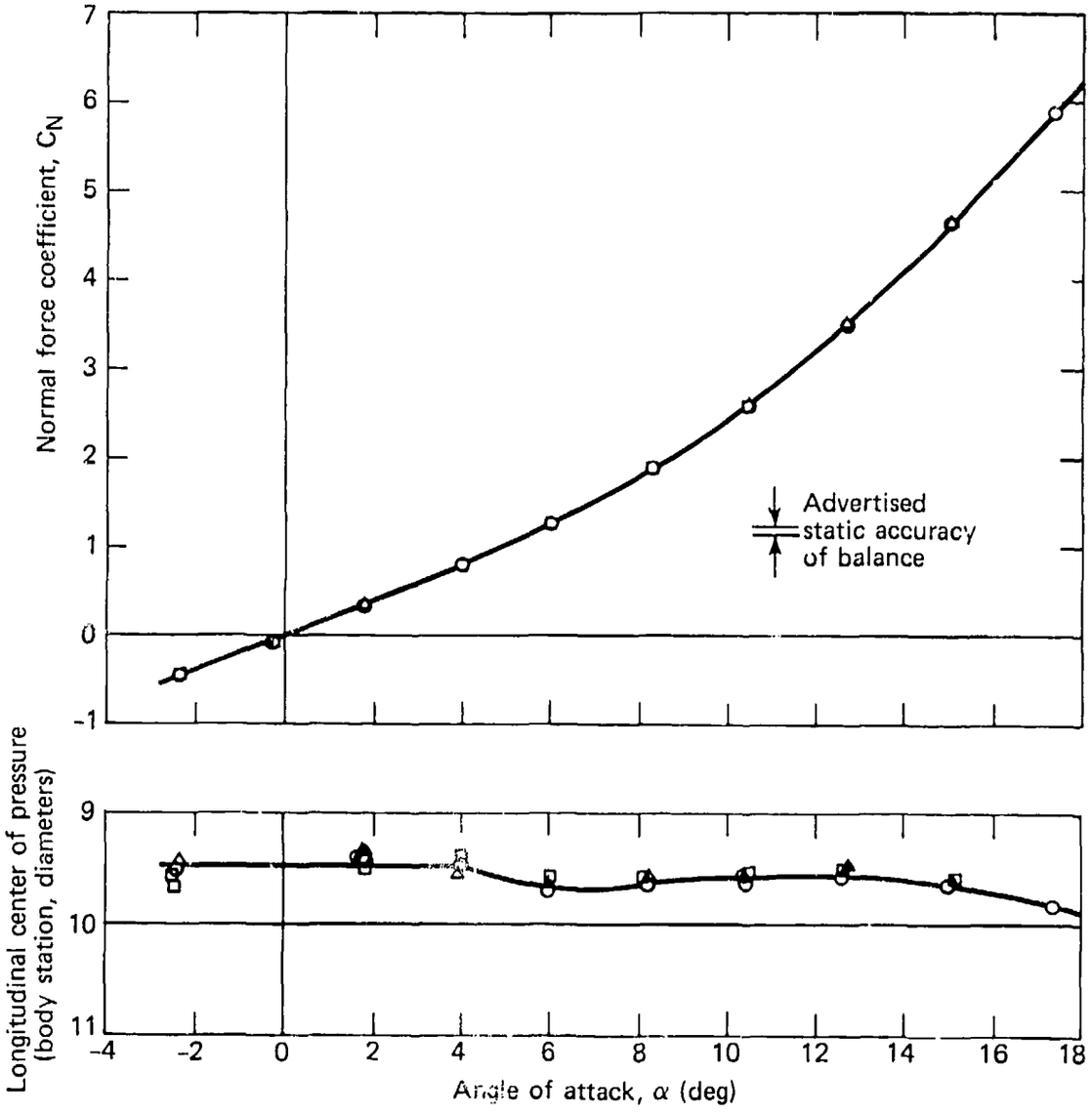

Fig. 3 Effect of roll rate on normal force coefficient and center of pressure travel.

M = 2.51

Sym	Run No.	$\dot{\phi}$ (Hz)	$\dot{\phi}$d/2V (rad)	Re x 10^{-6} (per ft)	i (deg)	Data sampling (pts/sec)
△	7	-17	-0.0046	8.8	0	240
○	5	-30	-0.0080	8.3	0	240
●	5	-9	-0.0024	8.3	0	240
□	6	-40	-0.0108	8.9	0	240

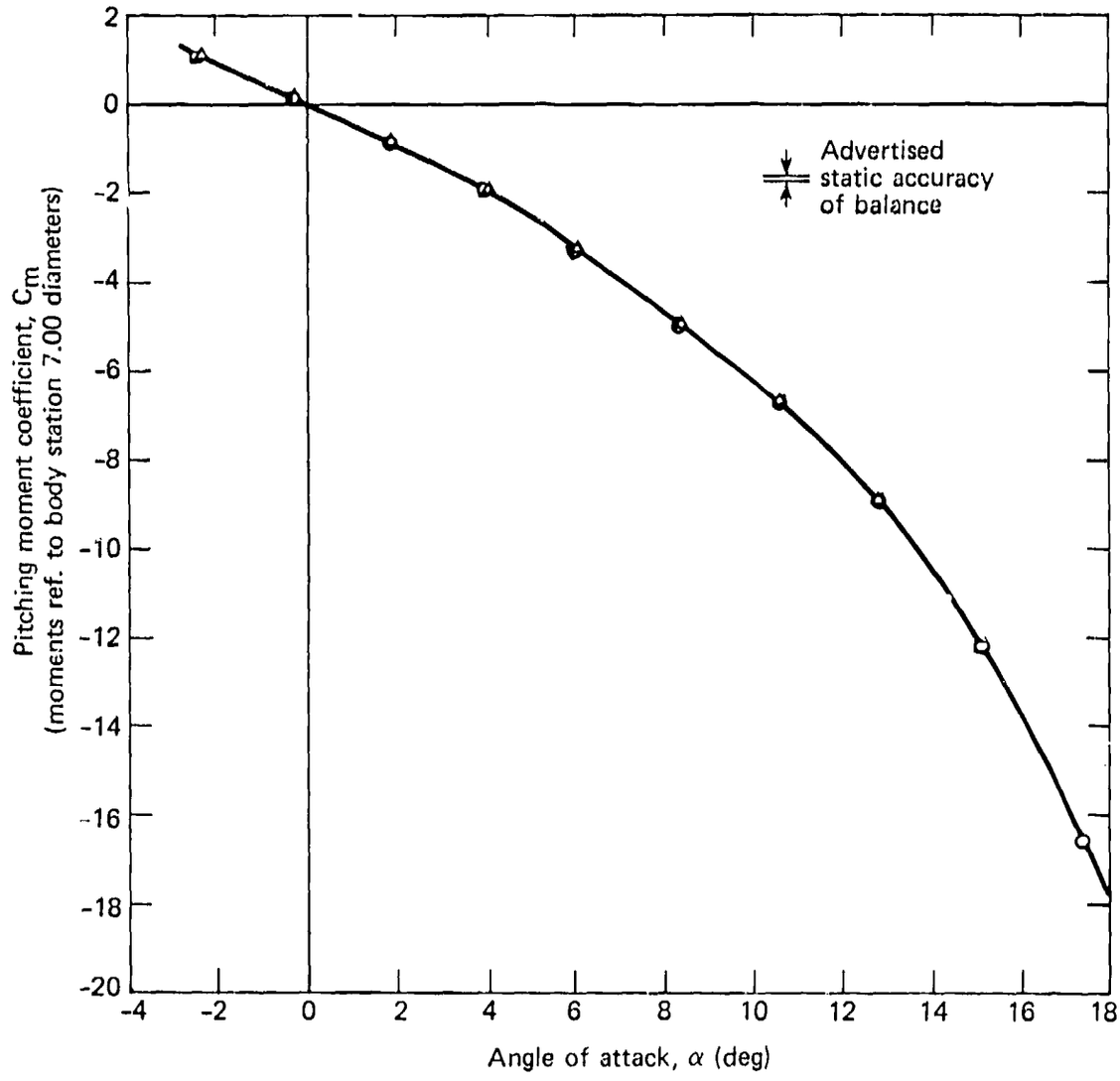

Fig. 4 Effect of roll rate on pitching moment coefficient.

M = 2.51

Sym	Run No.	$\dot{\phi}$ (Hz)	$\dot{\phi}d/2V$ (rad)	Re x 10^{-6} (per ft)	i (deg)	Data sampling (pts/sec)
△	7	-17	-0.0046	8.8	0	240
○	5	-30	-0.0080	8.3	0	240
●	5	-9	-0.0024	8.3	0	240
□	6	-40	-0.0108	8.9	0	240

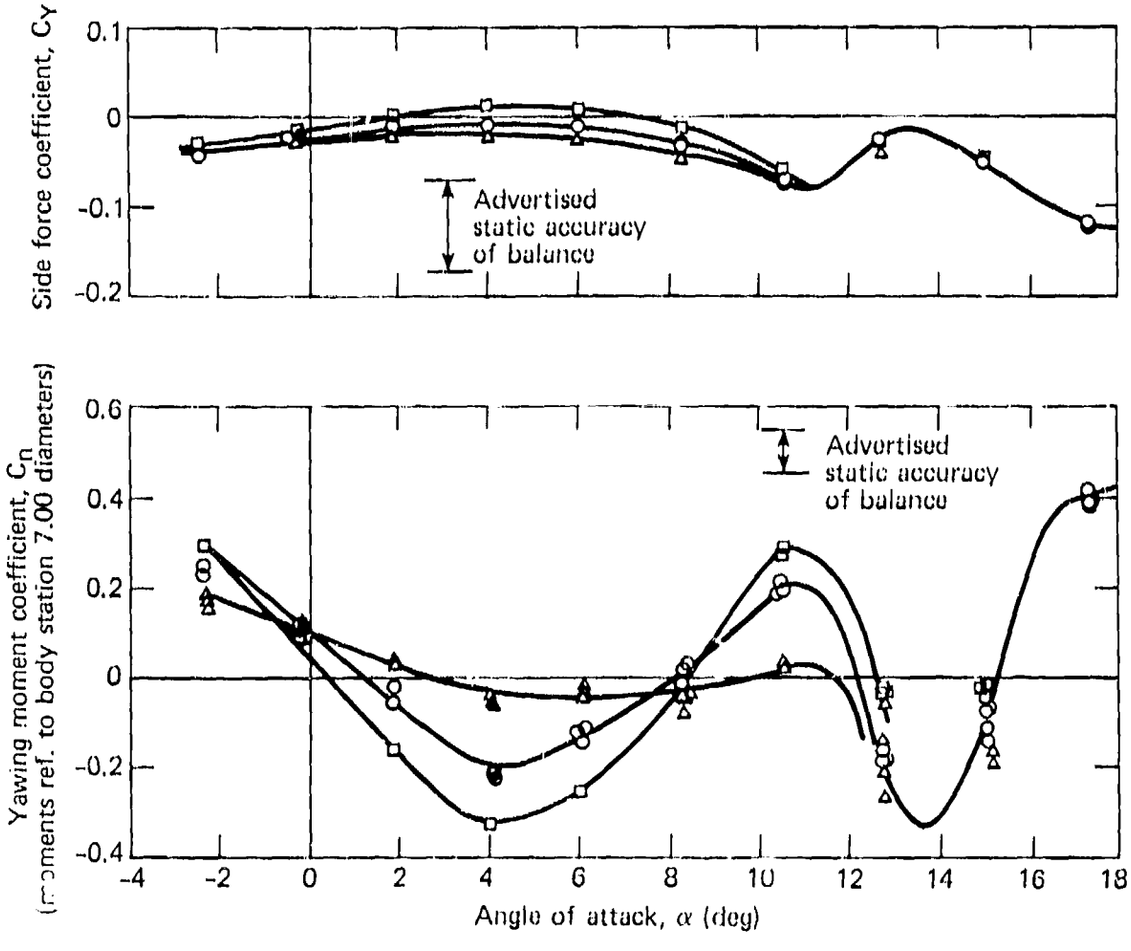

Fig. 5 Effect of roll rate on induced side force and yawing moment coefficients.

M = 2.51

Sym	Run No.	$\dot{\phi}$ (Hz)	$\dot{\phi}d/2V$ (rad)	Re × 10^{-6} / ft)	δ_s (deg)
□	14	-30	-0.0082		20
△	9	-30	-0.0081		10
○	5	-30	-0.0080	8.3	0
▽	13	-30	-0.0081	8.3	-10
◇	17	-30	-0.0081	8.5	-20

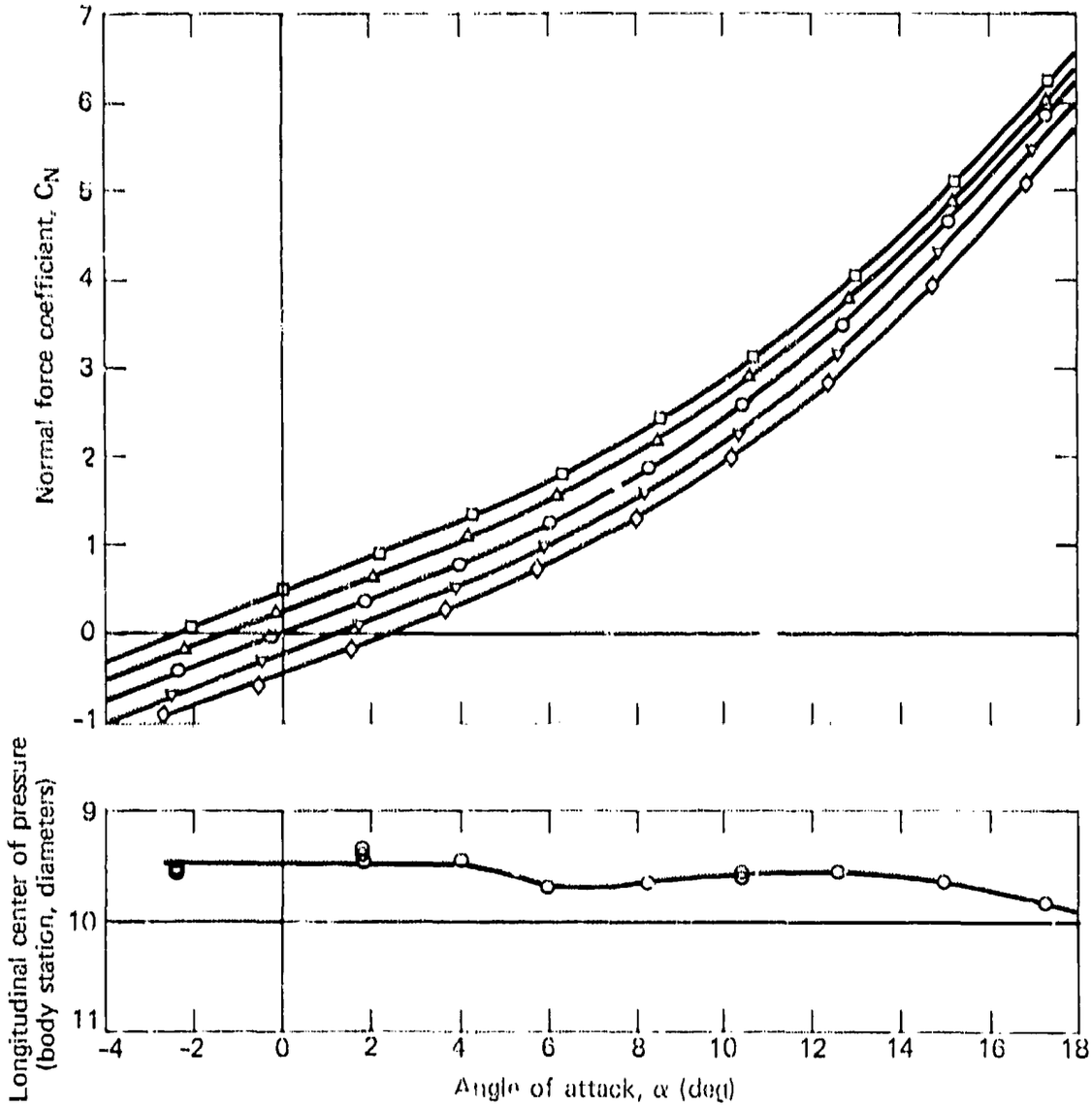

Fig. 6 Variation in normal force coefficient and center of pressure travel with angle of attack and steering deflection amplitude.

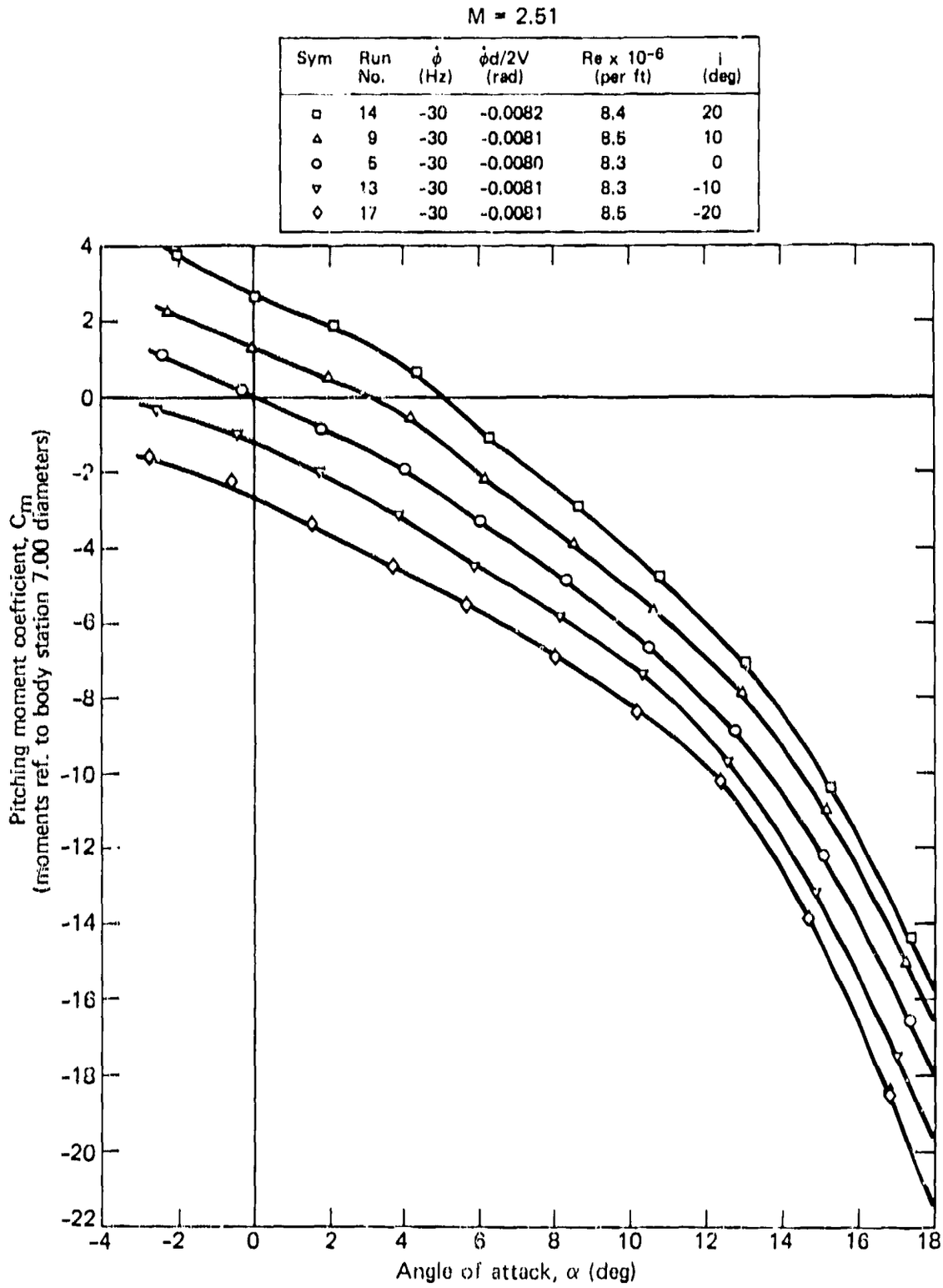

Fig. 7 Variation in pitching moment coefficient with angle of attack and steering deflection amplitude.

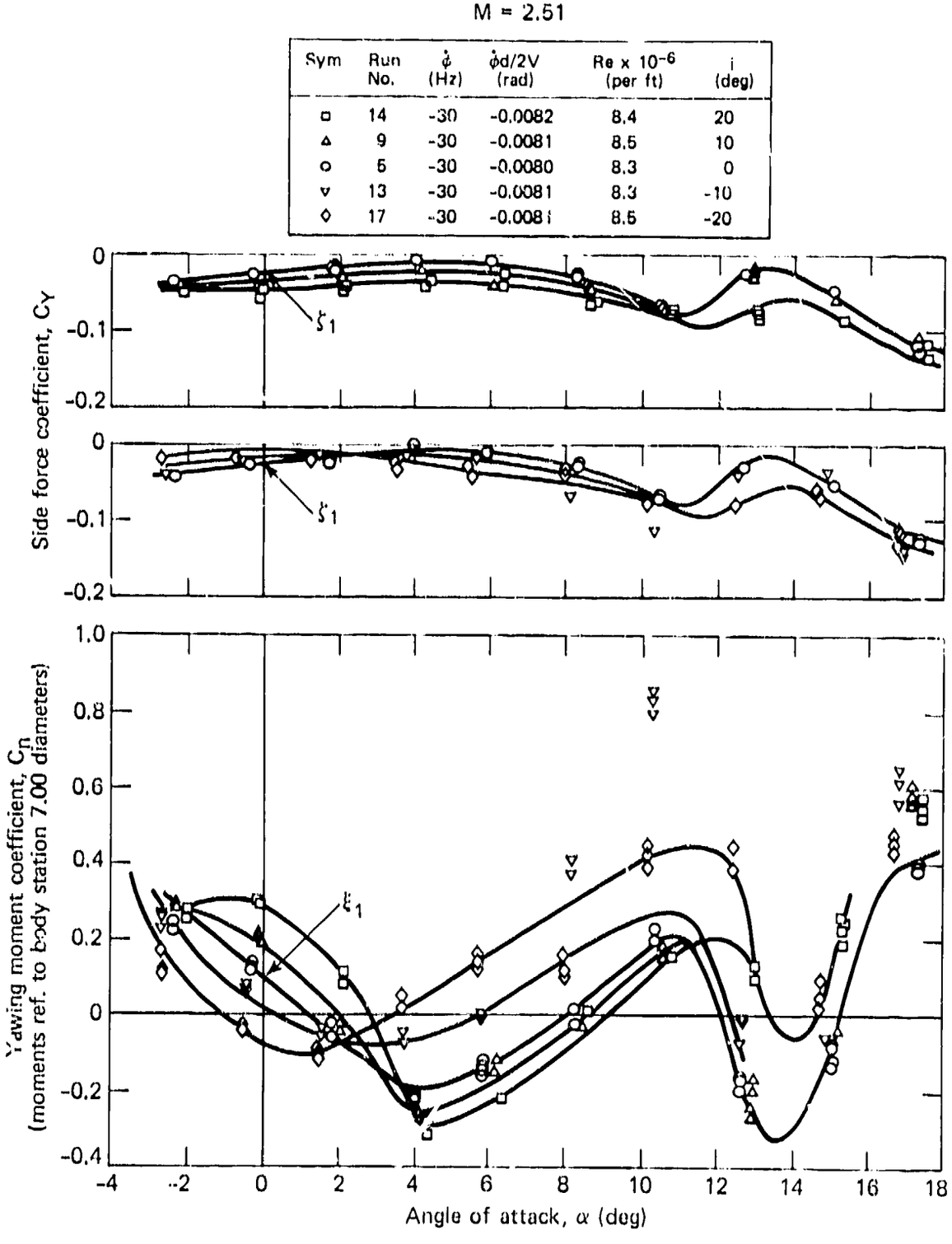

Fig. 8 Variation in induced side force and yawing moment coefficients with angle of attack and steering deflection amplitude.

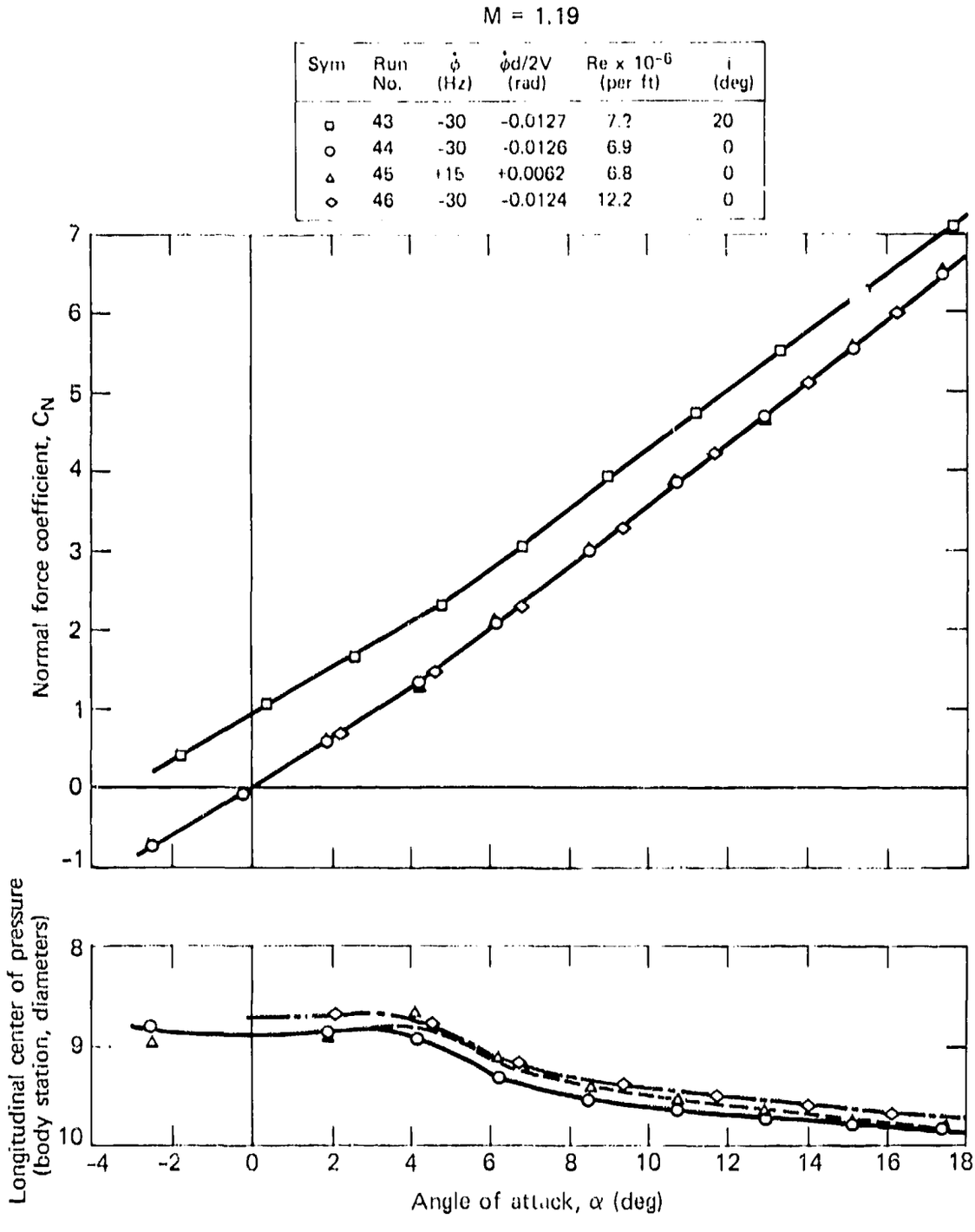

Fig. 9 Variation in normal force coefficient and center of pressure travel with angle of attack and steering deflection amplitude.

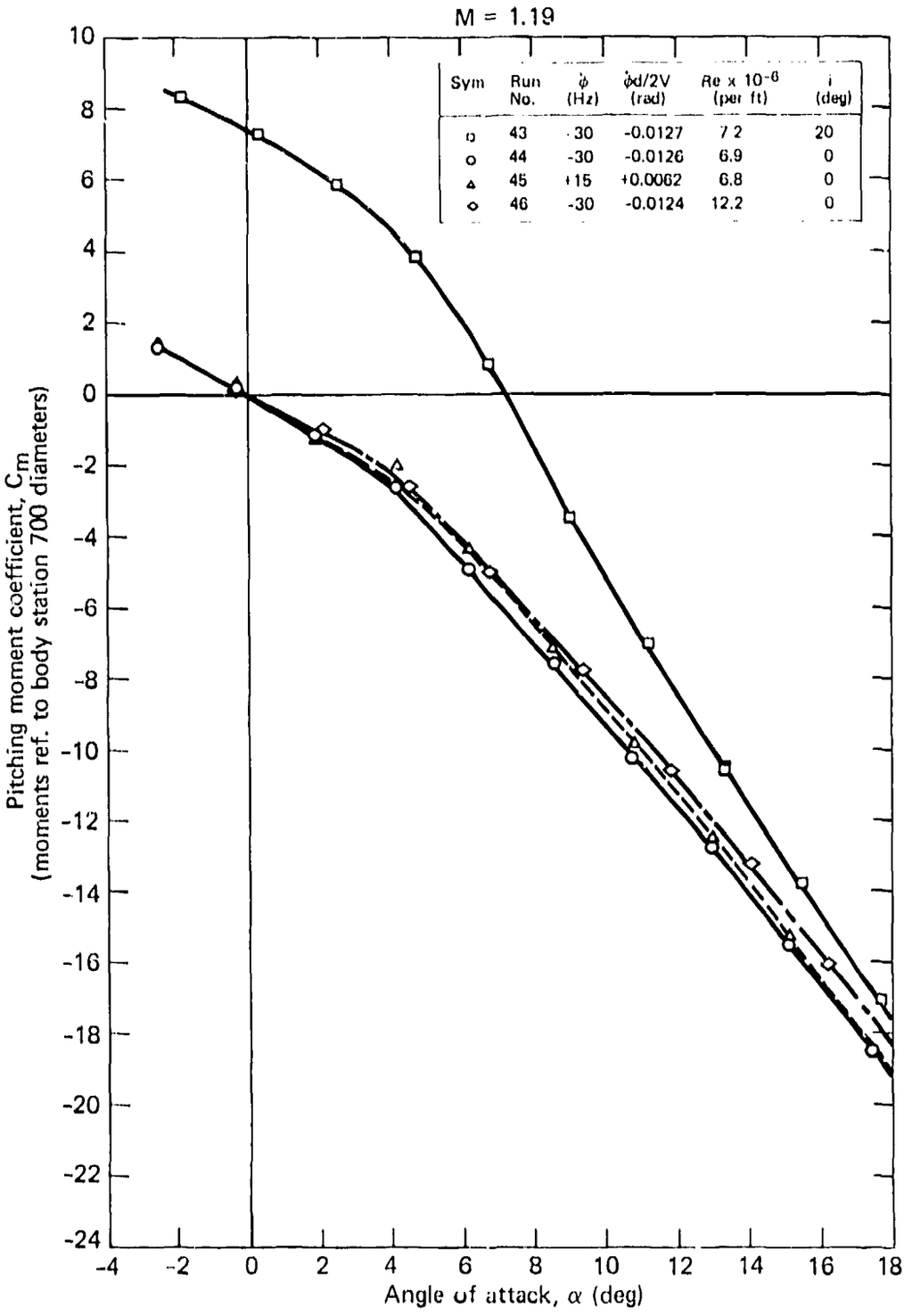

Fig. 10 Variation in pitching moment coefficient with angle of attack and steering deflection amplitude.

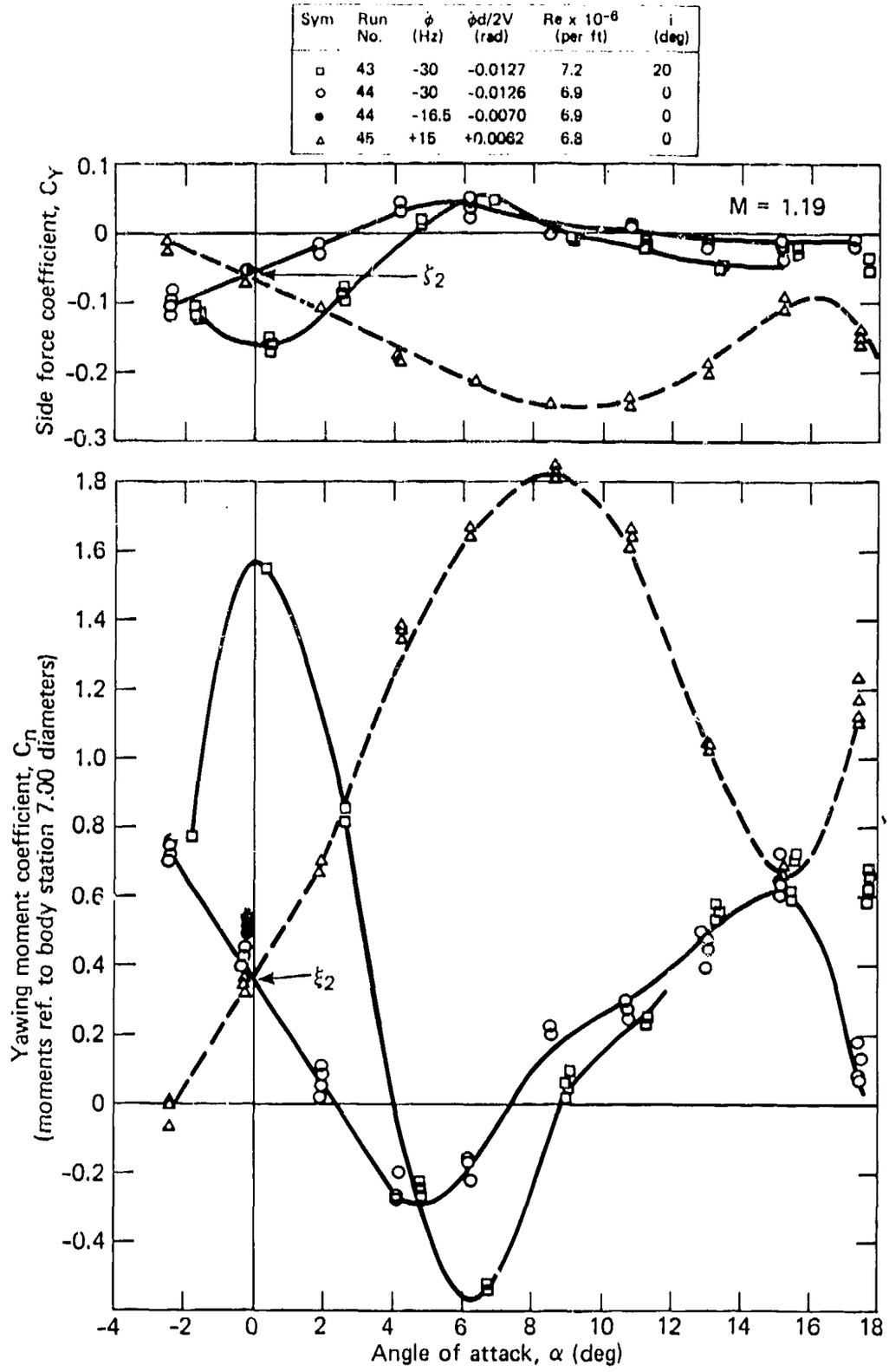

Fig. 11 Variation in induced side force and yawing moment coefficients with angle of attack and steering deflection amplitude.

M = 2.51

Sym	Run No	$\dot{\phi}$ (Hz)	$\dot{\phi}d/2V$ (rad)	Re x 10^{-6} (per ft)	i (deg)
△	7	-17	-0.0046	8.8	0
○	5	-30	-0.0080	8.3	0
●	5	-9	-0.0024	8.3	0
◇	8	-30	-0.0080	8.6	0
□	6	-40	-0.0108	8.9	0

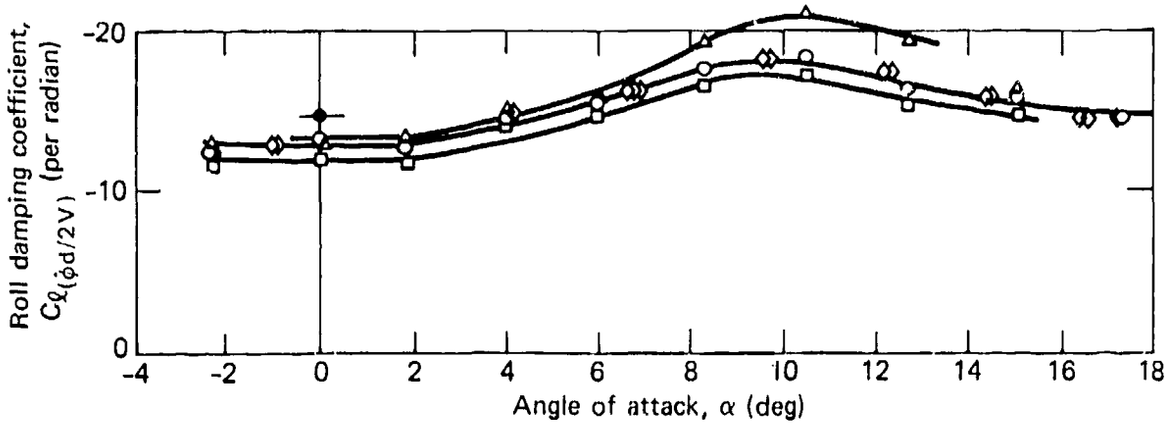

Sym	Run No.	$\dot{\phi}$ (Hz)	$\dot{\phi}d/2V$ (rad)	Re x 10^{-6} (per ft)	i (deg)
□	14	-30	-0.0082	8.4	20
△	9	-30	-0.0081	8.5	10
○	5	-30	-0.0080	8.3	0
▽	13	-30	-0.0081	8.3	-10
◇	17	-30	-0.0081	8.5	-20

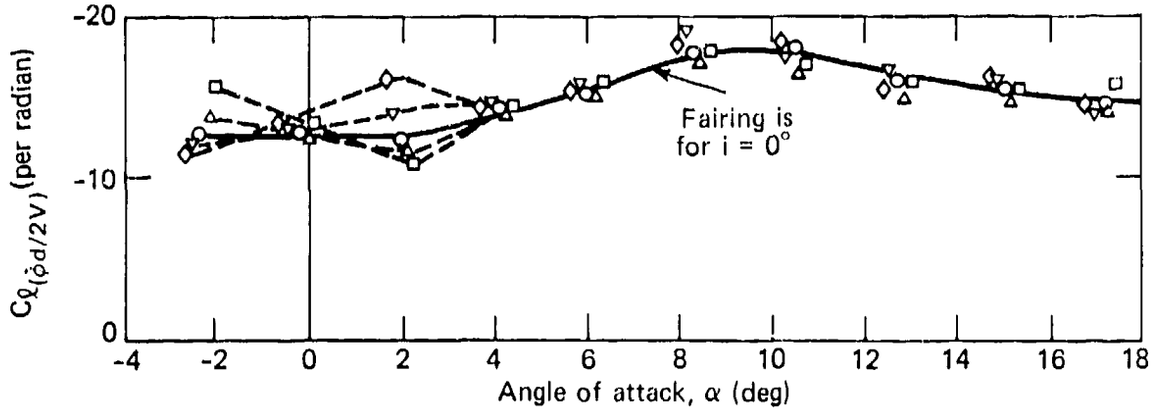

Fig. 12 Calculated roll damping characteristics.